Complex Planetary Systems II: Latest Methods for an Interdisciplinary Approach
Proceedings IAU Symposium No. 382, 2024
A. Lemaitre & A.-S. Libert, eds.
doi:10.1017/S1743921323004003

Medium Earth Orbit Secular Resonances and Navigation Satellites

Edoardo Legnaro

University of Padova. Department of Mathematics "Tullio Levi Civita"
Aristotle University of Thessaloniki. Department of Physics
email: edoardo.legnaro@gmail.com

Abstract. Inclination-only dependent lunisolar resonances shape the dynamics of MEO (Medium Earth Orbit) objects over secular time scales (i.e. several decades). Their main effect is to increase an object's eccentricity, possibly up to a value where the orbit's perigee meets the Earth's atmosphere and friction will determine the object's re-entry. Thus, understanding this mechanism allows the design of low-cost end-of-life disposal strategies which exploit the resonant dynamics. In this proceeding, we will summarize our results in developing an analytic theory for lunisolar resonances and the characterization of diffusion properties along them. On this topic, the techniques proposed are of interest in most problems of secular resonances encountered in Celestial Mechanics.

Keywords. Diffusion, Lunisolar Resonances, Navigation Satellites

1. Introduction

The MEO (Medium Earth Orbit) region spans from an altitude of 2000 km up to the Geosynchronous orbit, 35786 km, and is the home of various artificial satellites. Among those, we have the GNSS (Global Navigation Satellites System) constellations: the European GALILEO ($a \sim 29600$ km, $i \sim 55°$), the American GPS ($a \sim 26560$ km, $i \sim 55°$) the Chinese BEIDOU ($a \sim 27906$ km, $i \sim 55°$) and the Russian GLONASS ($a \sim 25510$ km, $i \sim 64.8°$). As many studies have highlighted, the MEO region is characterized by the presence of a network of secular lunisolar resonances which govern the dynamics (see Rosengren et al. (2015), Daquin et al. (2016), Daquin et al. (2022), Legnaro and Efthymiopoulos (2022) and references therein). A *lunisolar secular resonance* occurs whenever

$$\exists\, \vec{k} = (k_1, k_2, k_3) \in \mathbb{Z}^3 \backslash \{0\} \qquad \text{s. t.} \qquad k_1 \dot{\omega} + k_2 \dot{\Omega} + k_3 \dot{\Omega}_L = 0, \tag{1}$$

where ω and Ω are respectively the argument of perigee and node of the satellite, while Ω_L is the node of the Moon. If $k_3 = 0$, the resulting resonances are independent of a and e and thus are located at a critical value of the inclination $i_\star$ found by solving

$$k_1 \left(5 \cos^2 i - 1\right) - 2 k_2 \cos i = 0. \tag{2}$$

So, these resonances are called *inclination-only dependent lunisolar resonances* (or ILSRs). The main effect of such resonances is to increase an object's eccentricity, potentially up to a value so high that the orbit's perigee reaches the atmosphere and then friction determines the re-entry (see Figure 1 and Rossi (2008), Alessi et al. (2014), Gkolias et al. (2016), Alessi et al. (2016), Armellin and San-Juan (2018) and Skoulidou et al. (2019)).

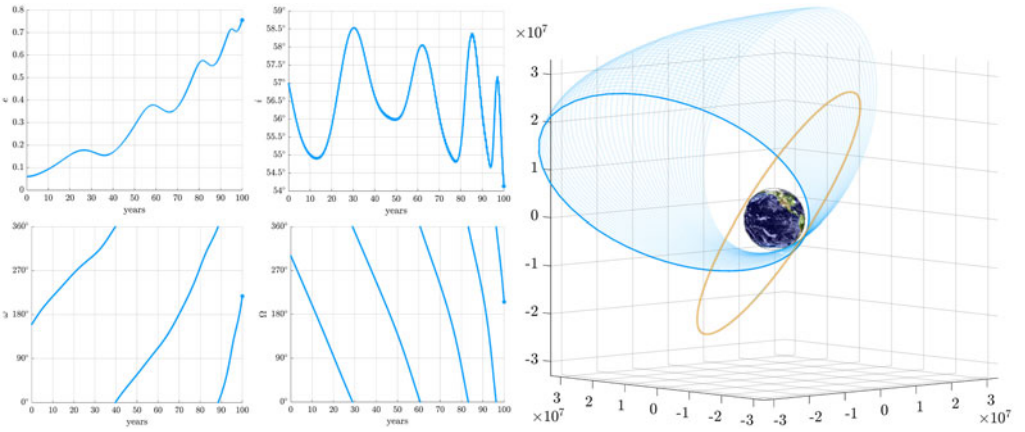

Figure 1. Numerical integration of a satellite at Galileo altitude with $A/m = 0.01$, $a = 29600$ km, $e = 0.06$, $i = 57°$, $E = 10°$, $\omega = 160°$, $\Omega = 300°$. The orbit is propagated using a cartesian integrator in the EME2000 reference frame. Left: evolution of the Keplerian elements e, i, ω, Ω. Right: 3D view of the satellite's orbital plane in cartesian Earth-centered coordinates with axis' unit in km at time $t = 100$ years, with initial circular inclined orbit portrayed in orange and trace showing the orbital position over the previous year, with solid blue line indicating the final orbit. From an almost circular orbit, in 100 years the satellite's eccentricity grows to a value where the satellite's perigee reaches the Earth's atmosphere, so that drag starts the satellite's decay. The minimum lifetime τ of a satellite in the resonant domain of the $2g + h$ resonance approximately follows a logarithmic law, and an object with these initial conditions would have $\tau = 168$y for $e_0 = 0.01$, $\tau = 262$y for $e_0 = 0.001$, $\tau = 369$y for $e_0 = 0.0001$. More details on this can be found in Legnaro (2023).

Nevertheless, as highlighted by these numerical studies, the MEO region and graveyards of navigation satellites are unstable, meaning that a slight difference in initial conditions may lead to dramatically different evolutions of the eccentricity.

This is the reason why having an analytic theory that can provide insights into finding which initial conditions will lead to the re-entry of an object can allow the design of low-cost end-of-life strategies for navigation satellites and space debris.

This proceeding is structured as follows. In Section 2, we will outline the steps needed to study a given lunisolar resonance. In Section 3, the Melnikov and Landau-Teller theories will be presented as a tool to obtain semi-analytical estimates of the speed of chaotic diffusion for an ensemble of points moving in the domain of a lunisolar resonance. In addition, such an approach can be useful in most problems encountered in Celestial Mechanics where a system is driven by the separatrix-like stochastic layers of a secular resonance, such as the ν_6 secular resonance between asteroids and Saturn or secular resonances in the main belt. Finally, Section 4 will summarize the results presented.

2. Analytic Theory for Secular Lunisolar Resonances

The details of our results on the development of an analytic theory for secular lunisolar resonances in the MEO region can be found in Daquin et al. (2022) and Legnaro et al. (2023).

The steps needed to study a given lunisolar resonance are the following. We first derive a set of resonant variables (J_R, u_R, J_F, u_F) adapted to the particular resonance at hand, which involves a 'fast' and a 'resonant' component. This allows to derive a Resonant Hamiltonian $H_R(X, Y, J_F, u_F, A, \Omega_L)$, having Poincaré variables X, Y and a dummy action A conjugated to the node of the Moon Ω_L. Finally, by finding a suitable analytic approximation of the fast component we arrive at an integrable Hamiltonian H which

https://doi.org/10.1017/S1743921323004003 Published online by Cambridge University Press

• allows us to understand and predict the structures seen in Fast Lyapunov Indicator (FLI) cartography while changing the initial values of Ω_L or of the satellite's perigee and node ω, Ω,

• provides insights into the eccentricity growth mechanism, allowing to understand the different behaviours of the maximum eccentricity reachable along a lunisolar resonance as a function of the initial phases and eccentricity,

• allows to reliably predict the domain of lunisolar resonances.

In particular, if we define the *center manifold* as the normally hyperbolic invariant manifold where the motion of circular orbits takes place, it is possible to see that this manifold has a large measure of invariant tori, and the initial choice of Ω shifts the resonance along the tori limiting its domain. The initial choice of Ω_L changes the shape of the center manifold. We define *fast drift plane* (FDP) as the locus of points where the fast action J_F is constant. The (i, e) plane is foliated by FDP, and each FDP is associated with an integrable phase portrait which shows the resonance's separatrix. The combination of the initial values of ω and Ω defines a scanning direction, and its intersection with the integrable separatrix gives an eccentricity value for that specific fast drift plane. In addition, for every FDP, the extension of the figure-8 separatrix dictates the theoretical maximum eccentricity value e_{max} that an object would reach moving along the resonance. This can explain numerical results that find different behaviours of the maximum eccentricity as a function of the initial inclination and node, like Alessi et al. (2016).

3. Diffusion along lunisolar resonances

What can be done to characterize the diffusion properties of an ensemble of points along a lunisolar resonance? In Legnaro et al. (2023), we show how it is possible to find estimates on the diffusion speed adopting Melnikov or Landau-Teller approaches. Also, the presented framework can be applied to most secular resonances encountered in Celestial Mechanics.

The integrable model derived in Section 2 for lunisolar resonances belongs to the Second Fundamental Model of Resonance (SFM, see Henrard and Lemaitre (1983)). To illustrate the concepts of the theory, consider the following 'archetype model' for lunisolar resonances

$$H_a = -S\cos 2\sigma + S^2\lambda\left[1 + \varepsilon\cos(2\sigma - \phi) + \varepsilon\cos(2\sigma - \phi_2)\right] + A\Omega + A_2\Omega_2, \tag{3}$$

where $(A, A_2) \in \mathbb{R}^2$, $S \geq 0$, $\sigma \in \mathbb{S}^1$, and $\varepsilon, \Omega, \Omega_2 \geq 0$. Consider Poincaré variables $X = \sqrt{2S}\sin\sigma$, $Y = \sqrt{2S}\cos\sigma$. In systems like this, which involve a resonant degree of freedom coupled to oscillators, the evolution of the adiabatic actions is not uniform in time, but rather proceeds with a sequence of discrete 'jumps' (see Figure 2). The adiabatic action A captures the evolution of the energy of the system over time, thus we wish to model the diffusion on this variable.

Consider N trajectories $A_i(t)$. If the evolution of the i-th trajectory proceeds as a sequence of consecutive discrete jumps $\Delta A_i^{(j)}$ with mean period $< T >$, then there are $n = [t/ < T >]$ jumps taking place per each trajectory. Setting the initial condition $A_i(0) = 0$ for all $i = 1, \ldots, N$, we have

$$A_i(t = n < T >) = \sum_{j=1}^{n} \Delta A_i^{(j)}. \tag{4}$$

If the jumps are not correlated, i.e., the individual jumps $\Delta A_i^{(j)}$ are randomly chosen from a distribution $p(\Delta A)$ with mean $\mu = 0$ and dispersion $\sigma_{\Delta A}$, then by the central limit theorem follows $A_i \sim \mathcal{N}\left(0, n\sigma_{\Delta A}^2\right)$ for n large. Since $\mu = 0$, we have $\sigma_{\Delta A}^2 = < \Delta A^2 >$.

https://doi.org/10.1017/S1743921323004003 Published online by Cambridge University Press

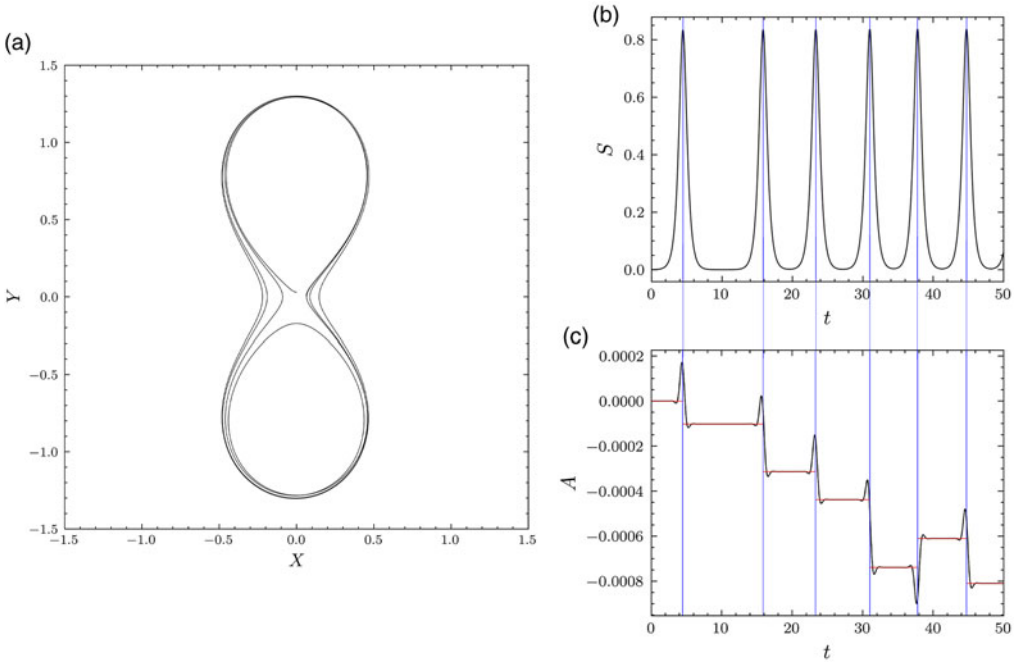

Figure 2. Evolution of an orbit with initial conditions $(X_0, Y_0) = (0, 0.3)$ and $(A, A_2, \phi, \phi_2) = (0, 0, 0, 0)$ under the flow of Hamiltonian (3) with parameters $\varepsilon = 0.01, \lambda = 1.2, \Omega = 5, \Omega_2 = \sqrt{5}$. The jumps in the adiabatic action A (c) correspond to homoclinic loops in the X, Y variables (a), and the jumps occur at the top of the loop, as can be seen from the evolution of $S(t)$ (b) which essentially measures the distance from the center.

Hence, the linear diffusion coefficient for the ensemble satisfies the relation:

$$D = \frac{n\sigma^2_{\Delta A}}{n < T >} = \frac{< \Delta A^2 >}{< T >} \tag{5}$$

In this way, the task of estimating the diffusion speed reduces to finding an estimate of $< \Delta A^2 >$ and $< T >$. For the first quantity, it is possible to adopt a *Melnikov Approach*. Consider $\dot{A} = -\frac{\partial H}{\partial \phi} = -\varepsilon\lambda S^2 \sin(2\sigma - \phi)$. We approximate $S(t)$, $\sigma(t)$, as well as $\phi(t)$, $\phi_2(t)$, with the analytic solution $\hat{S}(t)$, $\hat{\sigma}(t)$, $\hat{\phi}(t)$, $\hat{\phi}_2(t)$ of the separatrix of H_a for $\varepsilon = 0$. This yields

$$A(t) \approx A(t_0) - \int_{t_0}^{t} \varepsilon\lambda \hat{S}^2(u) \sin\left(2\hat{\sigma}(u) - (\phi(t_0) + \Omega u)\right) du. \tag{6}$$

The approximation is based on the idea that the evolution of the resonant variables (X, Y) (or (S, σ)) for initial conditions close to the separatrix of the integrable model is quite similar to the full one. Finally, the jump $\Delta A(\phi_0) = A(t_1) - A(t_0)$ between consecutive plateaus of $A(t)$ is approximated by the Melnikov integral

$$\Delta A \approx \Delta A_M = -\varepsilon\lambda \int_{-\infty}^{\infty} \hat{S}^2_\infty(u) \sin\left(2\hat{\sigma}_\infty(u) - (\phi_0 + \Omega u)\right) du. \tag{7}$$

In the particular example at hand, since $S_\infty(t)$, $\sigma_\infty(t)$ are odd and even functions of t respectively, we readily find:

$$\Delta A_M(\phi_0) = \varepsilon\lambda \sin\phi_0 I_1 \tag{8}$$

https://doi.org/10.1017/S1743921323004003 Published online by Cambridge University Press

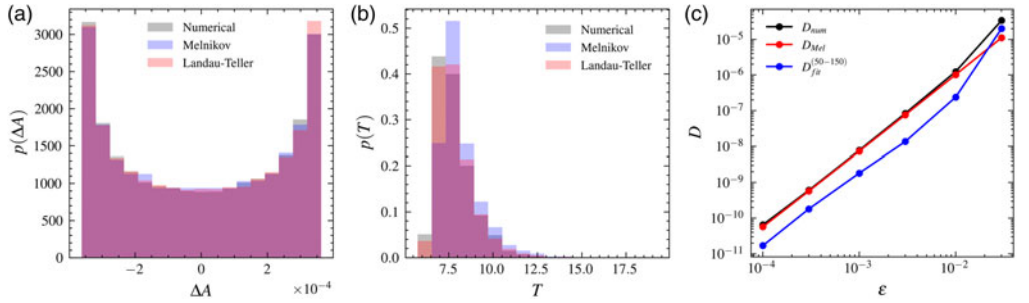

Figure 3. (a) Numerical (grey) histogram of the probability distribution $P(\Delta A)$ of the individual jumps in the value of the adiabatic action $A(t)$, collected by the data of the complete ensemble of 10000 simulated trajectories for $\varepsilon = 0.001, \lambda = 1.2, \Omega = 5, \Omega_2 = \sqrt{5}$ with initial X, Y data in the square $[-0.05, 0.05]^2$, on top of the corresponding histogram by the Melnikov approximation (blue, Eq.((8))). A third estimate of the same histogram (red) is obtained independently by the stochastic Landau-Teller model. (b) Comparison of the three histograms obtained as in (a) for the PDF of the periods $p(T)$. (c) The estimates on the diffusion coefficients with the assumptions of normal diffusion and uncorrelated phases $D = <\Delta A^2> / <T>$ for the numerical data (black) and by the Melnikov approach (red), as a function of ε. The blue curve shows the numerical diffusion coefficient as a function of ε obtained by linearly fitting the dispersion.

where

$$I_1 = \int_{-\infty}^{\infty} \hat{S}^2_{\infty}(u) \cos\left(2\hat{\sigma}_{\infty}(u) - \Omega u\right) du,$$

which in turn allows to find a theoretical estimate for the probability density function (PDF) of the jumps, which implies $<\Delta A^2_M> = \varepsilon^2 I_1^2/2$. Alternatively, a similar estimate of the PDF of the jumps can be found adopting what we call a *stochastic Landau-Teller model*, which consists of using the Fourier representation of finite-time homoclinic pulses along with a stochastic process based on random values of the integrable energy obtained through a suitably defined distribution.

For the mean period, it is possible to estimate the initial width of the chaotic layer by computing the *first subharmonic Melnikov integral*, which essentially computes the displacement between the stable and unstable manifolds of the hyperbolic point. Finally, it is possible to approximate $<T>$ by considering a uniform distribution of points inside the estimated chaotic layer and then computing for each point the analytic period.

It is now possible to estimate the diffusion coefficient with $D_{Mel} = \Delta A^2_M / <T>$, which approximates very well the numerically computed $D_{num} = <\Delta A^2> / <T>$ (see Figure 3 (a-b)). Still, in these systems, the presence of temporary stability islands and partial barriers generates long-term correlations of the 'phases' due to 'stickiness' effects (see Contopoulos and Harsoula (2010)). This can be addressed by introducing a *reduction factor* affecting all estimates on the speed of diffusion of the adiabatic actions given by the model, as also done in Chirikov (1979) (compare with Figure 3 (c)).

The same framework can be applied in the system of navigation satellites for the semi-analytical characterization of diffusion properties. We will focus on the $2g + h$ resonance since it is the most interesting for applications. We are interested in the diffusion along FDPs since they are linked to e_{max}, as discussed in Section 2. By averaging over the angles u_F and Ω_L of the resonant Hamiltonian and keeping just the leading terms, we get the integrable Hamiltonian which belongs to the SFM. Using the Melnikov approach and estimating the average period by computing the first subharmonic Melnikov integral, we obtain semi-analytically a diffusion coefficient

$$D(J_F)_M := \left\langle \Delta J_F^2 \right\rangle / \left\langle T \right\rangle \tag{9}$$

https://doi.org/10.1017/S1743921323004003 Published online by Cambridge University Press

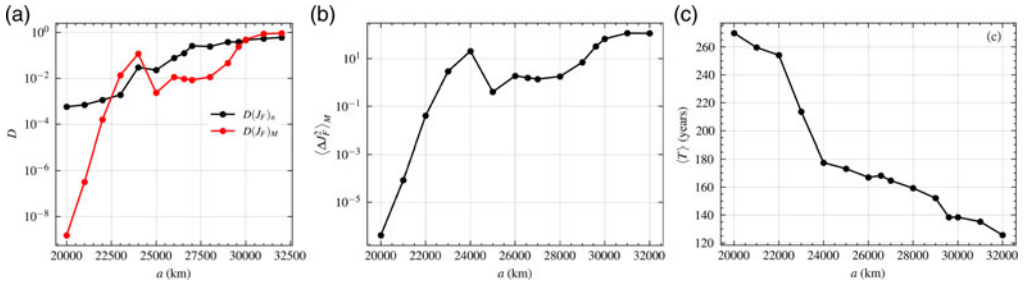

Figure 4. (a) Comparison between the semi-analytical diffusion coefficient $D(J_F)_M$ (red) and the numerically computed one $D(J_F)_n$ (black). (b) The value of $\langle \Delta J_F^2 \rangle$ is derived using the Melnikov approach. (c) The value of $\langle T \rangle$ estimated computing the first subharmonic Melnikov integral.

which can be compared with the numerically computed one $D(J_F)_n$ found by fitting the $\sigma^2(J_F)$ curve (see Figure 4).

The semi-analytical prediction works best for higher altitudes. This is to be expected, since lower altitudes would require additional normalization steps, while at higher altitudes no additional perturbation step would make the remainder smaller and so the original Hamiltonian is already the optional one.

4. Conclusions

In this proceding, we presented our results in the development of an analytic theory for secular lunisolar resonances. This allows to understand the dynamics of navigation satellites and so can be applied to the design of low-cost end-of-life disposal strategies. In addition, we provided a framework to semi-analytically characterize the diffusion in the MEO region. Such a framework can be applied to study the diffusion in most systems with secular resonances encountered in Celestial Mechanics.

References

Alessi, E. M., Deleflie, F., Rosengren, A. J., Rossi, A., Valsecchi, G. B., Daquin, J., & Merz, K. 2016, A numerical investigation on the eccentricity growth of GNSS disposal orbits. *Celestial Mechanics and Dynamical Astronomy*, 125(1), 71–90.

Alessi, E. M., Rossi, A., Valsecchi, G., Anselmo, L., Pardini, C., Colombo, C., Lewis, H., Daquin, J., Deleflie, F., Vasile, M., *et al.* 2014, Effectiveness of GNSS disposal strategies. *Acta Astronautica*, 99, 292–302.

Armellin, R. & San-Juan, J. F. 2018, Optimal Earth's reentry disposal of the galileo constellation. *Advances in Space Research*, 61(4), 1097–1120.

Chirikov, B. V. 1979, A universal instability of many-dimensional oscillator systems. *Physics reports*, 52(5), 263–379.

Contopoulos, G. & Harsoula, M. 2010, Stickiness effects in conservative systems. *International Journal of Bifurcation and Chaos*, 20(07), 2005–2043.

Daquin, J., Legnaro, E., Gkolias, I., & Efthymiopoulos, C. 2022, A deep dive into the $2g + h$ resonance: separatrices, manifolds and phase space structure of navigation satellites. *Celestial Mechanics and Dynamical Astronomy*, 134(1), 1–31.

Daquin, J., Rosengren, A. J., Alessi, E. M., Deleflie, F., Valsecchi, G. B., & Rossi, A. 2016, The dynamical structure of the MEO region: long-term stability, chaos, and transport. *Celestial Mechanics and Dynamical Astronomy*, 124(4), 335–366.

Gkolias, I., Daquin, J., Gachet, F., & Rosengren, A. J. 2016, From order to chaos in Earth satellite orbits. *The Astronomical Journal*, 152(5), 119.

Henrard, J. & Lemaitre, A. 1983, A second fundamental model for resonance. *Celestial mechanics*, 30(2), 197–218.

https://doi.org/10.1017/S1743921323004003 Published online by Cambridge University Press

Legnaro, E. & Efthymiopoulos, C. 2022, A detailed dynamical model for inclination-only dependent lunisolar resonances. Effect on the "eccentricity growth" mechanism. *Advances in Space Research*,, S0273117722006871.

Legnaro, E., Efthymiopoulos, C., & Harsoula, M. 2023,. Semi-analytical estimates for the chaotic diffusion in the second fundamental model of resonance. Application to Earth's navigation satellites.

Legnaro, E. A. 2023,. *Orbital Dynamics and Diffusion at the resonances in the near-Earth space environment*. PhD thesis, Aristotle University of Thessaloniki.

Rosengren, A. J., Alessi, E. M., Rossi, A., & Valsecchi, G. B. 2015, Chaos in navigation satellite orbits caused by the perturbed motion of the Moon. *Monthly Notices of the Royal Astronomical Society*, 449(4), 3522–3526.

Rossi, A. 2008, Resonant dynamics of medium earth orbits: space debris issues. *Celestial Mechanics and Dynamical Astronomy*, 100(4), 267–286.

Skoulidou, D. K., Rosengren, A. J., Tsiganis, K., & Voyatzis, G. 2019, Medium Earth Orbit dynamical survey and its use in passive debris removal. *Advances in Space Research*, 63(11), 3646–3674.